UC San Diego
UC San Diego Previously Published Works

Title

Three-Dimensional Reconstruction of Icosahedral Particles—The Uncommon Line

Permalink

Journal

Journal of Structural Biology, 116(1)

ISSN

Authors

Fuller, SD
Butcher, SJ
Cheng, RH
et al.

Publication Date

1996

DOI

Peer reviewed

Three-Dimensional Reconstruction of Icosahedral Particles—The Uncommon Line

S. D. FULLER AND S. J. BUTCHER

The Structural Biology Programme, European Molecular Biology Laboratory, Meyerhofstrasse 1, D-69012 Heidelberg, Federal Republic of Germany

AND

R. H. CHENG AND T. S. BAKER

Structural Studies, Department of Biological Sciences, Lilly Hall of Life Sciences, Purdue University, West Lafayette, Indiana 47907

Received May 15, 1995, and in revised form June 20, 1995

  The past few years have seen an explosion in the number of viral structures determined by icosahedral reconstruction from cryoelectron micrographs. The success of this work has depended upon a combination of the high-fidelity but low-contrast information contained in these images with efficient algorithms for determining particle orientation and three-dimensional structure. This review describes the principles behind the most commonly used method of reconstruction of the icosahedral particles and the method's implementation in an icosahedral reconstruction program suite.   © 1996 Academic Press, Inc.

ICOSAHEDRAL RECONSTRUCTION AND CRYOELECTRON MICROSCOPY

The advent of cryoelectron microscopy has allowed the imaging of isolated symmetric particles in the absence of stain and under conditions which preserve their symmetry. The image of a field of randomly oriented, symmetric particles in the absence of stain and under conditions which preserve their symmetry can be processed to yield a three-dimensional structure by determining the relative positions of the symmetry elements. This approach has been most powerful when applied to icosahedral particles because of their very high symmetry (point group 532—6 fivefold axes, 10 threefold axes, and 15 twofold axes for a total of 60 symmetry elements). This high symmetry eases the determination of the positions of the symmetry elements in individual images. It also decreases the number of images required to determine a three dimensional structure completely to a given resolution.

Icosahedral reconstruction from cryoelectron micrographs nicely complements X-ray crystallographic structure determinations. Orientation of the high-resolution structure of the virus capsid or an isolated protein within the reconstructed density yields an atomic model (Cheng *et al.,* 1995, 1994; Grimes *et al.,* 1995; Ilag *et al.,* 1995; Olson *et al.,* 1993; Smith *et al.,* 1993a,b; Stewart *et al.,* 1993). This approach provides a functional context for the X-ray structures of isolated proteins and allows more precise identification of molecular interactions. Cryoelectron microscopy in combination with image reconstruction also extends X-ray crystallographic studies because it can be applied to dynamic processes (Fuller *et al.,* 1995) and heterogeneous populations (Vénien-Bryan and Fuller, 1994) which would otherwise be inaccessible to structural study.

This discussion focuses on the modifications to the icosahedral reconstruction programs made over the past decade to allow their use for cryoelectron micrographs. We will not repeat the original description of the algorithms (Crowther, 1971).

The central problem in performing an icosahedral reconstruction is the reliable determination of the orientation of the individual particles. A particle of unknown structure is oriented on the basis of its icosahedral symmetry (Fig. 1—steps 1,2). Once putative orientations are determined for several particles, their transforms can be compared (Fig. 1—step 3) and the correct relative hand determined. These orientations are then used to combine the particle transforms to generate a symmetric three-dimensional transform and a symmetrized density (Fig. 1—step 4). This density can then be

used as a model to generate more reliable orientations for other particles in the input data (Fig. 1—step 5).

COMMON LINES

The determination of the orientation of a novel icosahedral particle is based on the symmetry elements. We use a polar coordinate system to describe the orientations (Fig. 1) in which a twofold axis lies along z, the adjacent threefolds along the x axis, and the adjacent fivefolds along y. One threefold view is ($\Theta = 69.09°$, $\Phi = 0°$) in these coordinates. A third angle, Ω, indicates the rotation of the view in the plane of projection. Our standard icosahedral asymmetric unit is the one-sixtieth of orientation space shown in Fig. 1 which is bounded by two fivefolds (for example 90°, 31.717° and 90°, −31.717°) and an adjacent threefold (69.09°,0°). A particle viewed down, for example, the threefold symmetry axis can be readily identified by the threefold symmetry of the projection. The same symmetry is seen in the Fourier transform of the projection which is a central section of the three-dimensional transform (DeRosier and Klug, 1968) taken normal to the direction of projection.

The common lines arise when the symmetry axis is not along the direction of view. Applying a symmetry operation around this symmetry axis to the Fourier transform of the projection (Fig. 2A) gives rise to a second, identical plane which intersects the original plane along a line (Fig. 2B). Application of the inverse of this symmetry operation generates a third identical plane which also intersects the original and the second (Fig. 2C). These lines of intersection are common to the three symmetry-related planes of the transform and so have identical values. The construction in Fig. 2C shows the relative positions of the three planes in space for a threefold axis, and the three common lines. Only two lines of intersection are visible in the transform of the original plane of projection.
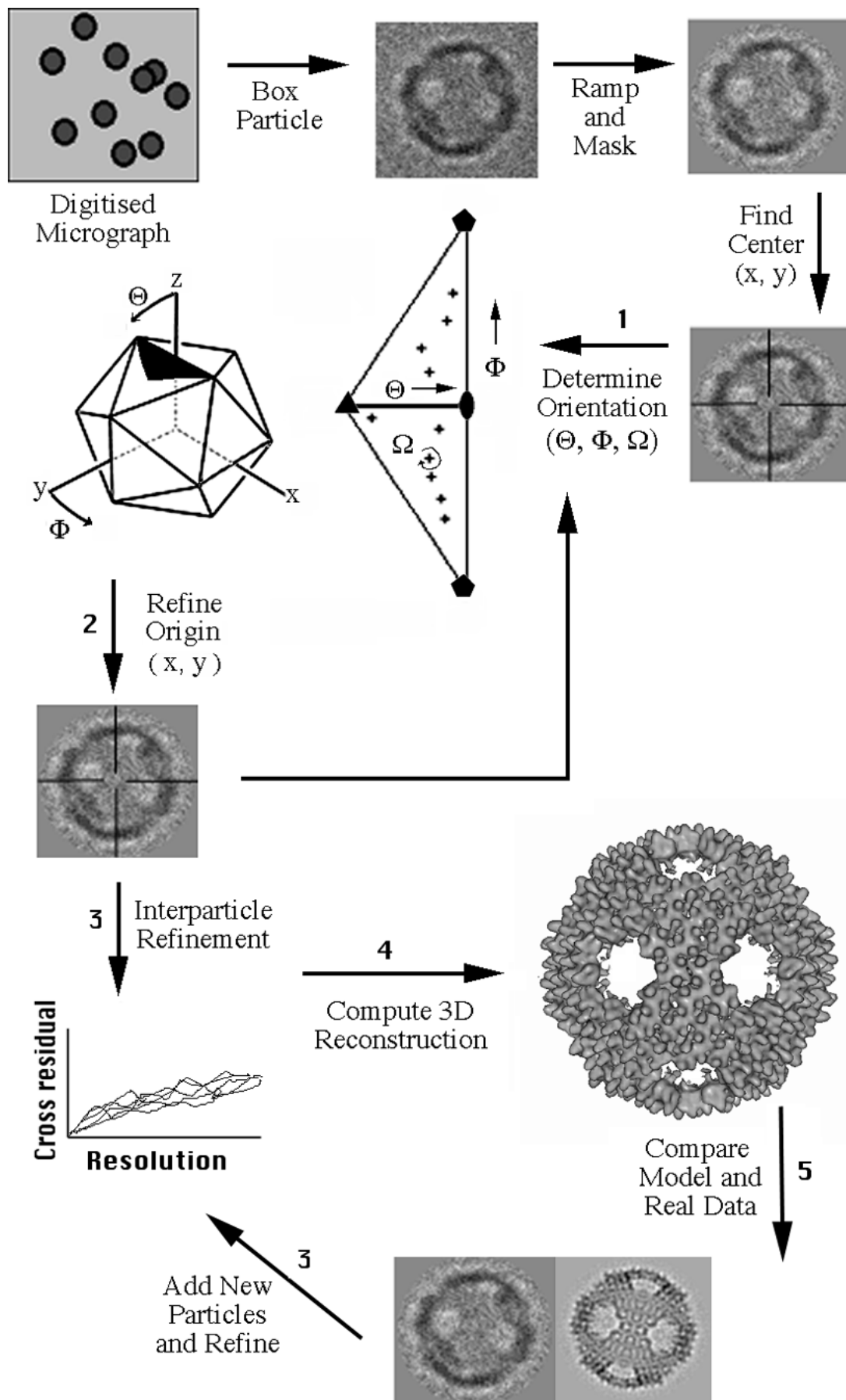
Each symmetry operation and its inverse about an axis generates a pair of common lines which lie to either side of the projection of the axis (Fig. 3). The existence of a symmetry axis at a particular position can be found by testing for equal values in the transform along the lines which would be generated by that axis. This would be a very weak test, easily satisfied for a single symmetry axis. The power of this approach for icosahedral objects comes from the fact that the high symmetry of the icosahedron gives rise to 37 pairs of common lines: each of the 6 fivefolds gives rise to two pairs (from $2\pi/5, -2\pi/5$ and $4\pi/5, -4\pi/5$), each of the 10 threefolds generates 1 pair ($2\pi/3, -2\pi/3$) and each of the 15 twofolds a further pair ($\pi, -\pi$) which lie along the projection of the twofold symmetry axis. The "pair" of common lines

generated by a twofold axis are colinear and force this line to be centrosymmetric ($\rho (x, y) = \rho (-x, -y)$) or equivalently forces the phases along this line in the transform to be 0 or π.

The existence of common lines is independent of the details of the structure; however, their usefulness in orientation is dependent on the presence of angular variation in the projection. The projections of a smooth object will show little angular variation and so the correct orientation will yield common lines which agree only slightly better with the projection than incorrect orientations. Experience with cryoelectron micrographs indicates that this angular variation can be maximized by selecting particular resolution ranges in the analysis.

The test for agreement between common lines is the calculation of a phase residual between the transform values which lie on the pairs of lines. The simplest form of the orientation search is then the calculation of the sum of the phase residuals between the 37 pairs of common lines in 1° steps for each of the orientations in the asymmetric unit (132480 distinct orientations corresponding to 736 values of Θ and Φ ((69.09°, 0°), (70°, −1°) , . . . , (90°, 31), (90°, 31.717°)) times 180 values of Ω). The orientation which generates common line positions with the lowest sum of phase residuals is taken as the correct one. This approach works most effectively for comparison of putative orientations near the center of the asymmetric unit (such as 80°, 11°) which have well-spread common lines (Fig. 3). It does not work equally well for other orientations. When a view is along (69°, 0°) or near to a symmetry axis (89°, −1°), the common lines are not well separated and a low residual is less significant because it results from fewer independent values of the transform (Fig. 3). This degeneracy is particularly serious for cryoimages which have a relatively low signal to noise ratio. A weighting scheme is used to compensate for this degeneracy. Orientations with the same Θ and Φ but different values of Ω have the same spread of common lines. A reduced χ_ν^2 statistic in which the number of degrees of freedom is the number of independent transform values used in the calculation of the distribution of residuals for a given Θ and Φ as a function of Ω is used to determine the probability of the lowest residual for that Θ and Φ. This probability is used to weight the residual for comparison between different values of Θ and Φ (Fuller, 1987). This χ_ν^2 weighting scheme is far from perfect but it has been sufficient to serve as the first step in the reconstruction of several dozen virus structures.

Common lines are used in two other places in the reconstruction process. One is in the refinement of the phase origin (x,y). The calculation of the phase residual described above assumes that the center of

Digitised
Micrograph

Box
Particle

Ramp
and
Mask

Find
Center
(x, y)

1 Determine
Orientation
(Θ, Φ, Ω)

Θ z

Φ

Θ Φ

Ω

y   x

2 Refine
Origin
(x, y)

3 Interparticle
Refinement

4 Compute 3D
Reconstruction

Cross residual

Resolution

3 Add New
Particles
and Refine

Compare
Model and
Real Data   **5**

the transform lies at the center of symmetry of the particle. Initially this is taken as the center of mass of the projection and determined by cross-correlation with a circularly symmetrized average projection. This origin is usually adequate for the first attempt at an orientation search. Once this initial orientation search yields a putative orientation, a refined phase origin can be determined by minimizing the common lines residual for that orientation. This refined orientation is used for further orientation searches. The cycle of orientation search and origin refinement is continued until consistent values of Θ, Φ, Ω, x, and y have been determined for several particles.

ORIENTATION REFINEMENT

The third use of common lines in the reconstruction process comes in the comparison of transforms of different particles. Once the orientations of the projections of two particles have been determined, the position of the common line between the two projections can be calculated. Further, one can generate a set of 59 other intersections (1 for each symmetry element) between the symmetry-related planes generated from these projections. This gives rise to 60 pairs of lines, i.e., lines which should have matching values in the two transforms. The sum of the phase differences between these pairs of lines is a measure of the degree to which the two transforms represent projections of the same structure at the given orientations. Calculation of the sum of the cross-common lines residuals over the entire set of particles identifies those particles which agree poorly with the rest of the set. These particles may truly differ or may simply have incorrectly determined orientations. Once these outliers have been excluded, the orientations of the remaining particles can be refined by altering the orientation and origin parameters to minimize the cross-common lines phase residual over the whole set of particles. Expe-

rience shows that this refinement is slow, extremely sensitive to noise, and only successful if the particles in the set have values close to the correct ones.

An important aspect of refinement is the determination of a consistent hand for the particles. The projection of a particle will have an identical common lines residual for the orientation Θ, Φ, Ω and Θ, Φ, $\Omega + \pi$. These two orientations (unflipped and flipped) correspond to viewing the same particle from opposite directions or to the projections arising from the particle and its enantiomorph. Although the common lines residual for an individual particle is the same for these two orientations, the cross-common lines residual between the particle and another of fixed orientation will be different. Particles which exhibit strong enantiomorphic features at resolutions as low as 50 Å such as the papovaviruses (which have a handed triangulation number, T = 7d) show dramatic differences and allow a consistent set of orientations to be established quickly (Baker *et al.,* 1985, 1991). Particles such as herpes virus (T = 16) (Baker *et al.,* 1990; Booy *et al.,* 1991), adenovirus (T = 25) (Stewart *et al.,* 1991), or Semliki Forest virus (T = 4) (Vénien-Bryan and Fuller, 1994), for which only the structural unit shows handedness, show the difference only at higher resolutions (35 Å or finer). The proper hand for such a structure must be selected by trying all possible combinations of flipped and unflipped particles for the set. Since correct refinement is dependent on the selection of the proper hand for each particle, this hand selection must be repeated at each step of the refinement of the orientations. This is fairly compute intensive. A dynamic algorithm is used to speed the search for the best combination of orientations. The set of hand choices for a subset of particles is extended by including all possible orientations of an additional particle in each round and retaining only those sets which could generate a residual comparable to the best observed in previous rounds (Stewart *et al.,*

FIG. 1. Overview of the reconstruction process. The steps in a typical icosahedral reconstruction are depicted using images of SDS-treated bacteriophage PRD1. The processing of the images which precedes step 1 (boxing, ramping, masking, and centering) are accomplished with SPIDER (see Frank *et al.,* this issue). The icosahedral reconstruction program suite begins with 1—the common lines based orientation search (using the programs FFTRANS and EMICOFV), 2—origin refinement (EMICOORG), 3—interparticle refinement (SIMPLEX), 4—reconstruction (EMICOMAT, EMICOBG, EMICOLG, EMICOFB, SYMMETRIZE), and 5—model-based orientation search (PACK_MRC_IMAGE, EMPFTREF1). The corresponding programs in the PURDUE version of the icosahedral reconstruction program suite are: preprocessing—EMIMG; 1—EMFFT, EMICOFV; 2—EMICOORG2; 3—EMICOGRAD; 4—EMICOMAT, EMICOBG, EMICOLG, EMICOFB, EMICOSYM; and 5—EMIMG, EMPFT. The coordinate system used for describing orientations is shown in the second line of the figure. Capital letters are used to denote reciprocal space variables (Θ,Φ,Ω) and small letters (x,y) are used to denote real space coordinates. The asymmetric unit triangle is bounded by two fivefold axes (90°, ±31.717°) and a threefold axis (69.09°,0°) and is shown in a planar representation with the symmetry axes marked by pentagons and a triangle and on the surface of an icosahedron to show its relationship to the Cartesian axes. The twofold axis (90°,0°) between the fivefolds is shown with the standard crystallographic symbol. Refinement of the phase origin corresponds to changing the center of the area used to calculate the transform and hence is described in the real space coordinates (x,y). Orientation searches are done using the transform of the projection and hence the orientation is described in terms of the reciprocal space angles (Θ,Φ,Ω) which are numerically identical to their real space counterparts. The Purdue and EMBL versions of the icosahedral reconstruction program suite use different settings of the icosahedral axes. The EMBL setting is described in the text. The Purdue setting generates an equivalent asymmetric unit which is bounded by two fivefolds Θ,Φ = (31.717°, ± 90°) and the threefold at (20.91°,0°) and the twofold at (0°,0°); however, this is transparent to the user of either program set.
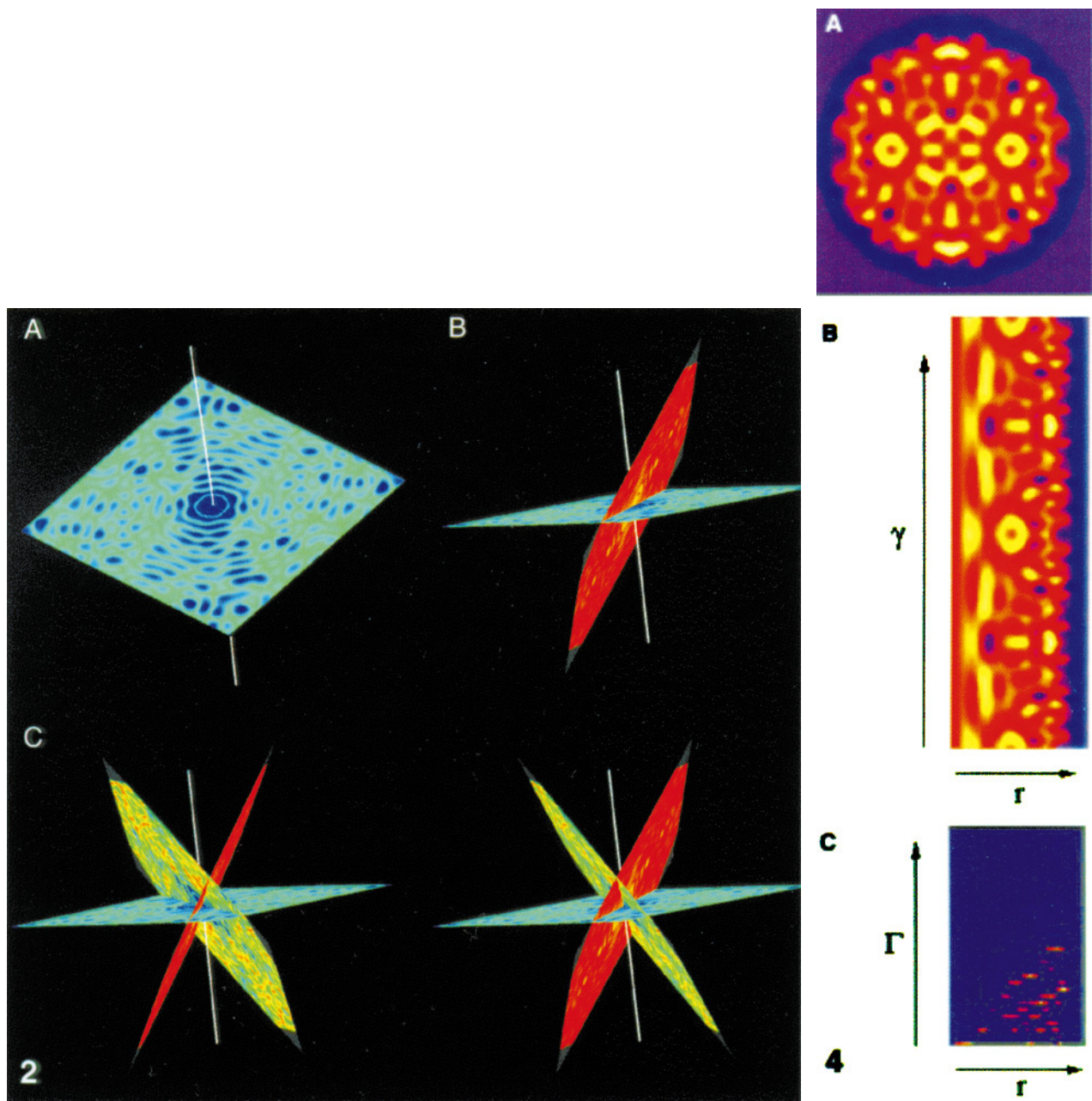
FIG. 2. Generation of common lines. The common lines are generated by the application of a symmetry axis which is not along the direction of view. The generation of common lines by a threefold axis is depicted here using the transform of an image of the enveloped bacteriophage PRD1. The direction of view (vertical white line) is near to the twofold axis ($\theta = 89°, \phi = -1°$). (A) The transform of the resulting projection. Rotations in Ω correspond to the rotation of this plane (a central section of the three-dimensional transform) around the view direction. (B) The symmetry-related plane generated by a 120° rotation around a threefold axis directed toward the reader. Application of a $-120°$ rotation around the same axis yields a third plane. The stereo pair of C shows the positions of the three resulting common lines at the intersections of these planes. All three have identical values but only two intersections with the original plane are seen in the transform of the original projection. Note that the common lines are spaced evenly around the threefold axis which generated them.

FIG. 4. The generation of the pft used in the model-based orientation search method. The polar Fourier transform is generated by projection of the model (A), radial sampling of the projection (B) to produce $\rho(r,\gamma)$, and transformation of the radially sampled projection along the angular direction (γ) to produce a pft which is a function of r and Γ (C). Multiplication of pfts corresponding to the image and evenly spaced model projections allow rapid identification of the most similar projection to the image and hence yield an orientation for the image (see Cheng *et al.,* this issue).
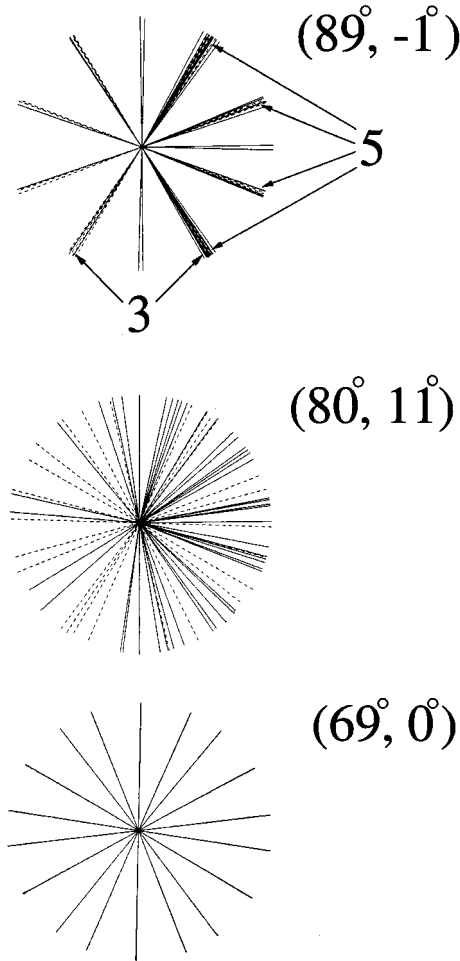
$(89°, -1°)$

5

3

$(80°, 11°)$

$(69°, 0°)$

FIG. 3. Distribution of the common lines for different orientations. The positions of the common lines are indicated for three orientations of an icosahedral particle. The situation corresponding to Fig. 2 is illustrated by the top panel ($\Theta = 89°, \Phi = -1°$). The positions of the pair of common lines generated by the threefold are marked with a large 3. The positions of the two pairs of common lines generated by a single fivefold axis are marked by a large 5. In each case the symmetry axis lies between the pairs. All 37 pairs of common lines are indicated for the three orientations. The common lines generated by the 15 twofold axes are shown as dashed lines since the two lines of the "pair" are colinear but oppositely directed. The Friedel symmetry of the transform forces the values along such a line to have phases of 0 or π. The change in the distribution and independence of the common lines for different orientations can be seen easily by comparison of the distribution near a twofold ($\Theta = 89°, \Phi = -1°$) or a threefold ($\theta = 69°, \phi = 0°$) to that near the center of the asymmetric unit ($\theta = 80°, \phi = 11°$). The positions of the common lines for different values of Ω are simply generated by rotating the positions for $\Omega = 0$ in the plane. Hence the distributions of lines for the same Θ and Φ but different Ω are similar.

1991). For larger sets of particles a simulated annealing approach is used (Metropolis *et al.*, 1953) in which the probability of flipping a particle in a cycle is an exponential function of the difference in residual between the flipped and unflipped orientation. Annealing is continued until further cycles result in no decrease in residual.

The refinement process is continued until a consistent hand has been established for all particles and the values of the common lines residual are acceptable for all the particles to the desired resolution. Sufficiently persistent refinement will result in improved residuals even for poor data sets. One can overcome this tendency to refine beyond the quality of the data by monitoring the free residual (Fuller *et al.*, 1995). Refinement of the data set is performed with a randomly selected subset of the cross-common lines. Once the refinement is completed for the subset, the values of the residuals are calculated for all of the common lines and compared to the those for the refined subset. If the refinement is proceeding properly, the orientations determined by refinement will also decrease the residual for the data left free during the refinement.

CALCULATING THE RECONSTRUCTION

The calculation of the reconstruction itself is the portion of the reconstruction process which has changed least since its original description (Crowther, 1971). The reconstruction is performed by determining the coefficients of a Fourier–Bessel expansion of the transform over a series of functions with 52 symmetry:

$$F(R, \Phi, Z) = \sum_n G_n(R, Z) \exp(in(\Phi + \pi/2)),$$

where the Z axis now corresponds to the position of the fivefold. This fivefold symmetry axis is imposed by including only those $G_n(R, Z)$ for which n is a multiple of 5. This method of imposing 52 symmetry is computationally efficient. The expansion coefficients $G_n(R, Z)$ are determined separately for each annulus of radius, R, and height, Z, in the transform. The orientation of each particle is used to determine the positions of the 59 planes equivalent to the original 1. For all orientations but the fivefold, each of these 60 planes will intersect an R, Z annulus at two positions (Φ_1, Φ_2). Combining the data from all 60 planes for all of the images gives a series of unevenly spaced sample points along each annulus. The coefficients of the expansion for each annulus are determined from the sample points by solving the linear equations

$$F_j = F(R, \Phi_j, Z) = \sum_n B_{jn} G_n(R, Z),$$

where the B_{jn} express the azimuthal dependence

$$(B_{jn} = \exp(in(\Phi_j + \pi/2))$$

for $G_n(R, Z)$. The number and spacing of the sample points limit the quality of the solution. This can be seen quantitatively in the eigenvalues of the least

squares solution. A low inverse eigenvalue indicates that many, well-spaced samples have been averaged to generate the coefficient, while a high one indicates that only a few sample points were used so that the coefficient is more susceptible to noise. The eigenvalue spectrum provides an answer to the question of how many images are necessary to determine a reconstruction to a given resolution. Since the eigenvalues are only determined by the spacing and number of the sample points, the eigenvalue spectrum is not affected by the signal to noise in the data or the reliability of the orientations. This information is seen from the resolution dependence of the phase residual during refinement.

Once the coefficients of the expansion of the transform are determined they are used to calculate the corresponding coefficients of the expansion in real space

$$g_n(r, Z) = \int_{-\infty}^{\infty} G_n(R, Z)\, J_n(2\pi Rr)\, 2\pi R\, dR$$

and the density in polar coordinates

$$\rho(r, \phi, z) = \sum_n \int_{-\infty}^{\infty} g_n(r, Z) \exp(in\phi) \exp(2\pi izZ)\, dZ.$$

This polar expansion is then interpolated onto a Cartesian system to complete the reconstruction process.

The symmetry of the expansion functions is 52 and hence the threefold symmetry elements of icosahedral (or 532) symmetry are not imposed on the reconstruction. Sixty icosahedrally related planes of data are extracted from each transform so that the presence of the threefold symmetry in the reconstruction signals agreement between the data from different particles. Full icosahedral symmetry can be imposed by real space averaging of the map. This averaging increases the signal-to-noise within the map.

In the early stages of a project, it is often useful to calculate a low-resolution, three-dimensional reconstruction from a single particle. The icosahedral sampling of the data forces such a reconstruction to be icosahedral but the eigenvalue spectrum will indicate that it is poorly determined and artifact rich as a result. Such a reconstruction can never serve as evidence for the icosahedral nature of the particle, but it can be useful in classifying particles or generating models for further orientation searches.

MODEL-BASED ORIENTATION SEARCHES

The reader who has never attempted to determine orientations by the use of common lines will have no appreciation of its difficulty or the lack of certainty which plagues the early steps in the reconstruction process. The development of a model-based orientation search method for icosahedral particles allows one to use a first, possibly noisy, reconstruction to check and refine orientations independently of the common lines approach (Cheng *et al.,* 1994). In the early stages of the reconstruction, the comparison of the two methods allows one to gain confidence in the correct orientations and discard incorrect orientations quickly. Once a structure has been established from a subset of data, the use of model-based refinement allows rapid screening for other additional particles and expansion of the data set.

The model-based refinement algorithm used in the icosahedral programs is based on a polar Fourier transform (pft) (Cheng *et al.,* this issue). A three-dimensional structure which has usually been symmetrized and radially cropped to increase its signal to noise ratio is used to generate projections for each value of θ and ϕ throughout the asymmetric unit (Fig. 4A). Each model projection $\rho(x,y)$ is then sampled onto polar coordinates $\rho(r,\gamma)$ (Fig. 4B). The density for each r is then Fourier transormed to produce the pft which is an array of one-dimensional Fourier transforms along γ (Fig. 4C). These pfts are used to select the projection which most closely matches the particle image. The conversion to pfts allows comparison which is independent of Ω. Each particle image is first centered by cross-correlation with the circularly averaged projection of the model and then converted to a pft. The best match between the model and the image is found by multiplication of the pfts to calculate the one-dimensional cross-correlation. The model orientation which gives the highest cross-correlation is selected. Once the best match of projection to image has been found, the best value of Ω is determined by interpolation in the polar cross-correlation function. The Ω is estimated by a parabolic fit to the peak of the one-dimensional cross-correlation function maps to a rotation since this is a polar Fourier transform. The hand is selected by cross-correlating the image with the unflipped and flipped model projections. The center of the image is then refined by using this model projection. The values of the new orientation and origin are then written out in a format which can be used by cross-common lines refinement or by a further round of model-based orientation search.

DATA FORMATS, OPERATING SYSTEMS, AND PROGRAM NAMES

The icosahedral reconstruction programs described above have their origin in a set of FORTRAN routines written by R. A. Crowther at the MRC LMB that have been modified and extended by a continuous interchange between the groups of EMBL and Purdue. The EMBL and Purdue versions are functionally equivalent but utilize different data formats

and program names. Both run under VMS on AXP and VAX architectures. The EMBL version utilizes the MRC image, map, and fft formats and has been ported to IRIX and to OSF1. An architecture stamp on the files allows their reading on either UNIX or VMS machines in the same manner that CCP4 files can be exchanged between architectures. The Purdue version utilizes a packed image format in which many images are stored in a single file. This helps minimize "bookkeeping" of files and reduces the overhead of many file openings. Only image data is stored. The fft is calculated within each program as it is needed.

FUTURE PROSPECTS

The programs now available cover a comprehensive set of manipulations for icosahedral reconstructions. The future holds the promise of increased resolution. Instrumental improvements such as the use of higher voltage electron microscopes and field emission guns are obviously one way to achieve this. However, as the resolution is increased, the number of particles used for averaging and the accuracy with which the particles need to be aligned also need to increase. These are computationally intensive tasks and are candidates for parallel computing algorithms. One recent important lesson is that improved image quality and larger data sets do indeed lead to higher-resolution structures. It is clear that the limit has not been reached and that the intrinsic order of the particles will support even higher resolution.

REFERENCES

Baker, T. S., Drak, J., and Bina, M. (1985) The structure of SV40 virus by electron microscopy of unstained frozen hydrated suspensions and negatively stained crystalline arrays, *Biophys. J.* **47,** 50a.

Baker, T. S., Newcomb, W. W., Booy, F. P., Brown, J. C., and Steven, A. C. (1990) Three-dimensional structures of maturable and abortive capsids of equine herpesvirus 1 from cryoelectron microscopy, *J. Virol.* **64,** 563–573.

Baker, T. S., Newcomb, W. W., Olson, N. H., Cowsert, L. M., Olson, C., and Brown, J. C. (1991) Structures of bovine and hu-

man papilloma viruses: Analysis of cryoelectron microscopy and three-dimensional image reconstruction, *Biophys. J.* **60,** 1445–1456.

Booy, F. P., Newcomb, W. W., Trus, B. L., Brown, J. C., Baker, T. S., and Steven, A. C. (1991) Liquid-crystalline, phage-like packing of encapsidated DNA in herpes simplex virus, *Cell* **64,** 1007–1015.

Cheng, R. H., Kuhn, R. J., Olson, N. H., Rossmann, M. G., Choi, H.-K., Smith, T. J., and Baker, T. S. (1995) Nucleocapsid and glycoprotein organization in an enveloped virus, *Cell* **80,** 621–630.

Cheng, R. H., Reddy, V. S., Olson, N. H., Fisher, A. J., Baker, T. S., and Johnson, J. E. (1994) Functional implications of quasi-equivalence in a T = 3 icosahedral animal virus established by cryo-electron microscopy and X-ray crystallography, *Structure* **2,** 271–282.

Crowther, R. A. (1971) Procedures for three-dimensional reconstruction of spherical viruses by Fourier synthesis from electron micrographs, *Philos. Trans. R. Soc. London* Ser. B **261,** 221–230.

DeRosier, D. J., and Klug, A. (1968) Reconstruction of three dimensional structures from electron micrographs, *Nature (London)* **217,** 130–134.

Fuller, S. D. (1987) The T = 4 envelope of Sindbis virus is organized by complementary interactions with a T = 3 icosahedral capsid, *Cell* **48,** 923–934.

Fuller, S. D., Berriman, J., Butcher, S. J., and Gowen, B. E. (1995) Low pH induces swiveling of the glycoprotein heterodimers in the Semliki Forest virus spike complex, *Cell* **81,** 715–725.

Grimes, J., Basak, A. K., Roy, P., and Stuart, D. (1995) The crystal structure of bluetongue virus VP7, *Nature* **373,** 167–170.

Ilag, L. L., Olson, N. H., Dokland, T., Music, C. L., Cheng, R. H., Bowen, Z., McKenna, R., Rossmann, M. G., Baker, T. S., and Incardona, N. L. (1995) DNA packaging intermediates of bacteriophage phiX174, *Structure* **3,** 353–363.

Metropolis, N., Rosenbluth, A., Rosenbluth, M., Teller, A., and Teller, E. (1953) Equation of state calculations by fast computing machines, *J. Chem. Physics* **21,** 1087–1092.

Olson, N. H., Kolatkar, P. R., Oliveira, M. A., Cheng, R. H., Greve, J. M., McClelland, A., Baker, T. S., and Rossmann, M. G. (1993) Structure of a human rhinovirus complexed with its receptor molecule, *Proc. Nat. Acad. Sci. USA* **90,** 507–511.

Smith, T. J., Olson, N. H., Cheng, R. H., Chase, E. S., and Baker, T. S. (1993a) Structure of a human rhinovirus-bivalently bound antibody complex: Implications for viral neutralization and antibody flexibility, *Proc. Nat. Acad. Sci. USA* **90,** 7015–7018.

Smith, T. J., Olson, N. H., Cheng, R. H., Liu, H., Chase, E. S., Lee, W. M., Leippe, D. M., Mosser, A. G., Rueckert, R. R., and Baker, T. S. (1993b) Structure of human rhinovirus complexed with F_{ab} fragments from a neutralizing antibody, *J. Virol.* **67,** 1148–1158.

Stewart, P. L., Burnett, R. M., Cyrklaff, M., and Fuller, S. D. (1991) Image reconstruction reveals the complex molecular organization of adenovirus, *Cell* **67,** 145–154.

Stewart, P. L., Fuller, S. D., and Burnett, R. M. (1993) Difference imaging of adenovirus: Bridging the resolution gap between X-ray crystallography and electron microscopy, *EMBO J.* **12,** 2589–2599.

Vénien-Bryan, C., and Fuller, S. D. (1994) The organization of the spike complex of Semliki Forest virus, *J. Mol. Biol.* **236,** 572–583.